

3D Surface Reconstruction and Change Detection of Miage Glacier (Italy) from Multi-date Archive Aerial Photos

Arsalan Malekian[1(✉)], Davide Fugazza[2], and Marco Scaioni[3]

[1] Politecnico di Milano, Lecco Campus, via G. Previati 1/c, 23900 Lecco, Italy
arsalan.malekian@mail.polimi.it
[2] Department of Environmental Science and Policy, Università Degli Studi di Milano, Via Celoria 2, Milan, Italy
davide.fugazza@unimi.it
[3] Department of Architecture, Built Environment and Construction Engineering, Politecnico di Milano, via Ponzio 31, 20133 Milan, Italy
marco.scaioni@polimi.it

Abstract. Historical aerial images provide valuable information for monitoring and change detection in different areas such as glaciers. Using aerial images, 3D models can be created and the geometry of the glaciers can be digitized manually to analyse their surface extent and evolution. Here, we use archive images to reconstruct 3D models of Miage glacier in the Val Veny region, Mont Blanc, Italy. First, the features of each dataset photos are inspected, and they are pre-processed to be used in the 3D reconstruction phase. This pre-processing is conducted to not only minimize the dataset's problems, including shadows covering the glaciers and insufficient image overlapping over crucial places, but also to generate the best achievable dense 3D point clouds from each dataset. Point clouds of reconstructed 3D models may be used to detect variations in the Val Veny region and determine the rate of retreat and height differences for each glacier in the area over time. This could be done by computation of distances between points in cloud pairs in consecutive years. In this phase, no manual shifting and translating of point clouds are required as they were georeferenced in the 3D reconstruction phase and automatically co-registered with Iterative Closest Point algorithm. Miage glacier in the Val Veny area was chosen to be assessed considering the quality of generated point cloud during the 3D reconstruction phase. The results of the comparisons indicate how the Miage glacier volume has varied throughout time. While volume changes of the evaluated glacier were almost negligible until the mid-1990s, investigations demonstrate a significant rise in volume decrease at the beginning of 21st century.

Keywords: 3D reconstruction · Photogrammetry · Change detection · Glacier monitoring · Archive aerial images

© The Author(s), under exclusive license to Springer Nature Switzerland AG 2022
O. Gervasi et al. (Eds.): ICCSA 2022 Workshops, LNCS 13379, pp. 450–465, 2022.
https://doi.org/10.1007/978-3-031-10545-6_31

1 Introduction

People and economic infrastructure in mountain areas are at risk as a result of natural processes related to the melting of glacier ice. Glacier avalanches, landslides, and slope instability produced by debuttressing, as well as catastrophic outburst floods from moraine-dammed lakes and outburst floods from glacier-dammed lakes, are examples of these phenomena [17]. The threat of cryospheric hazards as a consequence of climate change necessitates the implementation of preventive techniques [25]. Remote sensing is regarded as a valuable method for generating supporting data, such as Digital Elevation Models (DEM) and multispectral images. DEMs are especially effective for detecting glacier thickness and volume changes, as well as identifying steep places that are more susceptible to geomorphodynamic changes, such as mass movements [12].

Archive aerial photos, in particular, are one of the oldest data sources for glacier monitoring. Indeed, they are extremely useful for glacier observation in terms of extension, length, volume, and mass change [9]. In general, these archives consist of historical aerial photos collected for local topographic mapping projects based on photogrammetric techniques. In glaciological studies, they may be used to create geometrically precise 3D models of glaciers by using cutting-edge digital photogrammetric methods, such as Structure-from-Motion (SfM) and Multi-View Stereo (MVS) dense matching [13].

The majority of historical photos in the archives were captured by using analogue film cameras and then transferred onto digital images by photogrammetric scanners. Only in the two last decades, Digital Airborne Cameras (DAC) started to take over analogue cameras in order to directly record digital aerial imagery. Today the almost complete production in the photogrammetric market relies on the use of DACs.

Historic aerial photos were already used in the past to calculate comprehensive elevation and volume analyses. Sixteen Antarctic glaciers were analysed by using aerial photos since 1950s [10]. Between 1959 and 1990, DEMs and orthophotos were created for a glacier in Sweden based on consistent photogrammetric processing of aerial images [20]. Also, a dataset including scans of 300 (analogue) aerial images that were obtained between August and October of 1954 by the U.S. Air Force over the province of Trento was used for 3D modelling of glaciers and change analysis. The comparison between the 3D models of 1954 and 2015 showed changes up to 70–80 m in the height of glaciers in the region [24].

This paper investigates how historical aerial photos may be used to derive 3D models of Alpine glaciers, to be compared between different times in order to detect morphological and volumetric changes. The area of Val Veny in Aosta Valley (Northern Italy) is assumed as case study (see Sect. 2). Here some important glaciers are located, with the Miage Glacier being the largest one. Section 3 presents the adopted archive aerial photos that derive from the online repository of the National Geographic and Forestry Institute of France (IGNF). Sections 4 and 5 describe the methods applied for the photogrammetric 3D reconstruction and for comparing multi-temporal point clouds of glaciers, respectively. Results are shown and discussed in Sect. 6, while Sect. 7 draws some conclusions and addresses future work.

2 Study Area

This work is mainly focused on the evaluation of glacier changes in Val Veny area (see Fig. 1), which is located the Aosta Valley, a high elevation and relatively small administrative region in the Italian Western Alps (3,262 km^2). The Aosta Valley has the largest glacier coverage of any area in Italy, based on the latest Italian Glacier Classification [28]. There are 192 glaciers in the Aosta Valley Region with a total area of 133.7 km^2, accounting for 36 percent of the Italian glacier area (data from 2005–2011). The glaciers range in altitude from roughly 1400 to 4800 m a.s.l. [29].

Val Veny is a lateral valley of the Mont Blanc massif located west of Courmayeur town. This mountain valley is split into three sections: the section that runs parallel to the Mont Blanc massif between the Seigne pass (2,512 m a.s.l.) and part of the Miage Glacier, the middle part that is called Plan Vény, and the valley's entrance (1,444 m a.s.l.), which is surrounded by Mont Blanc and the lower Brenva Glacier [29]. The existence of significant geological components and varied outcropping lithologies, which are molded by glacial activity and result in a diverse geological environment, is an important aspect of this small region [13].

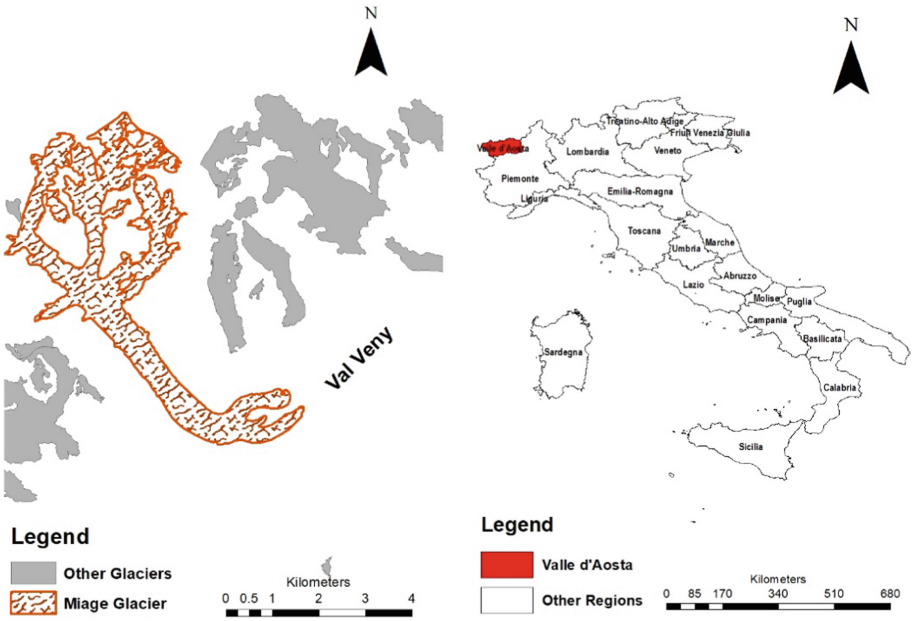


Fig. 1. Location of Aosta Valley in Italy and of Miage glacier among other glaciers of the region.

Miage Glacier are one of the primary glaciers in this area. It is the longest glacier in Italy and the largest debris-covered glacier in Europe, measuring roughly 10 km in length [7]. Debris covers approximately 5 km^2 out of its 11 km^2 total area, mostly from rockfall from neighbouring flanks and avalanching in deposition regions of its four tributaries [21]. Due to the quick thinning of the glacier tongue, debris transported

along within the glacier is also being exposed at an accelerated pace. The variety of supraglacial debris sources, as well as the peculiar mica schist-dominated lithology of the rock walls surrounding the glacier, results in a diverse debris lithology. The debris cover becomes continuous below 2,400 m a.s.l. and continues intact until the terminus. Crevasses or moulins, on the other hand, may cause inconsistent areas [26]. Although the spatial distribution of thicknesses is uneven, especially on sections of the northern terminal lobe, debris thickness usually increases between a few centimetres at 2,400 m a.s.l. to over 1 m at the terminus at 1,775 m a.s.l. [27].

Because of several key features, the Miage Glacier is the best example of a 'Himalayan Glacier of the Alps,' including its accumulation zone, steep cliffs characterised by avalanches, avalanches that indirectly feed the glacier, a notable difference in altitude between the accumulation area and the terminus, and variations in ice thickness in the frontal area [25].

3 Photogrammetric Data Description

The archive aerial photos used in this research over the Val Veny were obtained from multiple aerial missions operated from1967 to 2006. Images are provided in digital form through the WEB portal of the National Geographic and Forestry Institute of France (IGNF - *Institut National de l'Information Géographique et Forestière*). All datasets include a calibration certificate containing information on the camera and lens used (see Kraus 2008). Image orientation parameters computed after aerial triangulation or recorded by onboard GNSS/INS (Global Navigation Satellite System-Aided Inertial Navigation System) sensors are not generally provided, while mission information is generally limited to the average flight height, acquisition scale, and side overlap. Most missions were flown using analogue film cameras of different types, but all equipped with standard focal lens (150 mm) and film format (23 cm $\times$ 23 cm). Analogue panchromatic or colour photos were then transformed into digital using photogrammetric scanners. The selected pixel size was around 20 μm. Data sets collected in the last two decades (such as the one in 2006) were directly captured using a *frame* digital airborne camera (Table 1).

In all datasets, the variation of flying altitude is between 4.7 and 6.35 km, with photos from the 2001 dataset featuring the lowest flying height and the ones from 1967 showing the highest flying altitude, respectively. The coverage area of the photos from 1996 to 2001 is between 300 and 345 km^2, whereas the data from 1967, 1979, and 2006 cover an area of 132 to 173 km^2. Coordinates of camera perspective centres recorded by onboard GNSS are only provided for three datasets: 1996, 2000 and 2001. All of the photographs were acquired during the warmer months, from June to September, with the exception of the 1967 photos, which were taken in October.

The image quality was evaluated by taking into consideration some factors. Firstly, the aerial photographs completely encompass the Val Veny, particularly the glaciers. In flat, hilly, and mountainous locations, the ground coverage is acceptable for aerial triangulation and orthophoto generation. Secondly, the analogue photos were transformed into digital data after scanning, which degraded the image quality even further. [1]. The presence of steep terrain that characterize the mountains around Val Veny resulted in dark shadows on the photos (Fig. 2). Shadows frequently look as uniform black surfaces due to limited dynamic range [3]. Snow may also be a concern since it may smooth out the original terrain topography and create problems for image matching algorithms used for image orientation ad 3D surface reconstruction [31].

The information impressed on the lateral borders of each photograph is useful for a variety of objectives. The date and time of each set of images helps to better understand the dynamics of the glaciers by identifying the mean temperature in that region. The GNSS camera location could be used as approximation to help automatic image orientation [6], as described in the following section.

Table 1. Properties of dataset over Val Veny area from 1967 to 2006 downloaded from IGNF online repository.

Year	Date	No. images	Camera coordinate	Camera model	Flying Altitude [km]	Coverage area [km^2]
2006	Aug 23rd to Sep 5th	78	Not available	Digital	5.54	173
2001	Aug 1st to 13th	73	Available	RMKTOP15	4.78	345
2000	Jun 23rd to Aug 1st	25	Available	RMKTOP15	5.54	310
1996	Jul 3rd to Aug 4th	35	Available	RMKTOP15	5.02	301
1988	Jul 26th	23	Not available	RC10	6.15	321
1979	Sep 5th	19	Not available	RC10	5.7	144
1967	Oct 11th & 12th	24	Not available	RC10	6.35	132

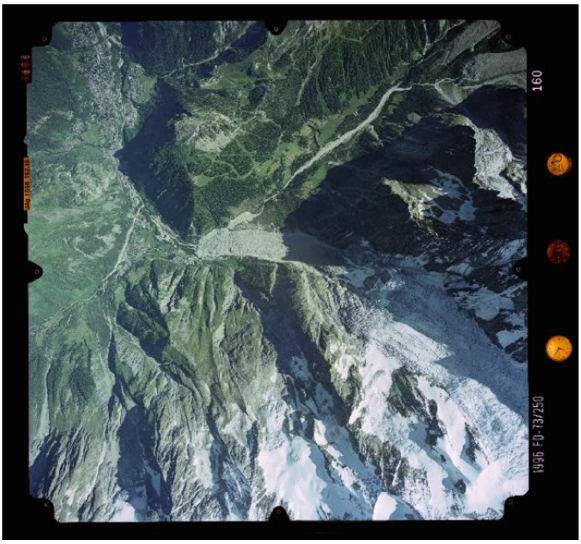


Fig. 2. Example of dark shadows on glaciers near vertical surfaces in 1996 image.

4 3D Model Reconstruction

The purpose of this work is to apply the described methodologies to reconstruct a 3D model from aerial historical photos over a 40-year period covering the Val Veny region. The photogrammetric procedure to reach this aim is presented in the following paragraphs.

4.1 Image Pre-processing

For categorization and editing, the images were loaded into Adobe Photoshop Lightroom Classic 9.4 release®. Lightroom is a professional-grade program for managing photography catalogues that is both affordable and user-friendly, in addition to having efficient processing algorithms [24]. The radiometric image balancing and adjustment was used in this investigation to mitigate differences in different photos due to different lighting conditions and presence of shadows. In all datasets the clarity and contrast are adjusted according to properties of the images. This procedure increases the capability of Structure-from-Motion and Multi-View Stereo matching techniques adopted for image orientation and dense point cloud generation [15].

4.2 Image Orientation

In this work 3D point cloud reconstruction has been performed by using a standard SfM and MVS approach, as implemented in the popular software package Agisoft Metashape® (www.agisoft.com). Agisoft Metashape® is a stand-alone software package that perform photogrammetric processing on digital photos and provides 3D spatial

data for use in different applications. Here, "Professional" version 1.7.5 of the software has been used.

The *image orientation* ("Alignment" in the software jargoon) is the initial phase in the process. During this phase, Images are sought for corresponding *keypoints* that are matched across images to create manifold *tie points* [11]. The availability of approximate values for camera stations (e.g., from onboard GNSS observations) may help speed up this process and limit the number of blunders. In the case these approximations are not provided, the image orientation process is applied first on sub-sampled low-resolution images, and then iteratively transferred to the ones at full resolution.

Tie points are then fed into a *bundle block adjustment* (BBA) internal module, which at the same time computes camera calibration parameters (including Inner Orientation and Additional Parameters for lens distortion compensation), Exterior Orientation (EO) parameters, and 3D coordinates of tie points. The latest ones are used to generate the "sparse point cloud" [8], that is then used to drive the successive dense matching phase [17]. Due to multiple overlapping of images, this step additionally assessed camera calibration and EO quality thanks to the data redundancy in the BBA. Prior to the more computationally intensive generation of dense point clouds, the user can assess precision and recognize problematic tie points using the sparse point cloud. The BBA solution was referred to an arbitrary reference system, since so far no ground constraints were included (e.g., ground control points).

4.3 Georeferencing

In order the define the coordinates of the output 3D point clouds in a mapping grid, some ground control points (GCPs) were needed. Unfortunately, GCPs were not measured in the archive photos from IGNF. To overcome the problem of georeferencing, natural features have been selected to serve as GCPs in stable areas over time and across all datasets, and their coordinates determined using accessible satellite data from Google Earth®. Even though in some regions of the area of interest the location of GCPs has been difficult if not impossible, GCPs have been selected to be well distributed in each photogrammetric block, avoiding weak configurations such as GCPs concentrated around the same line [25]. Typical stable objects within time are buildings and houses, that unfortunately are available only in villages and in the bottom part of the valley. Much more challenging has been to find stable parts in the upper parts of glaciers. The spots chosen to be GCPs are the same in all datasets, and 12 GCPs are considered in each dataset based on their availability.

Once a set of GCPs has been selected, a new BBA including their observations in the images has been run. Due to the low quality of measured GCPs, corresponding ground coordinated have been properly weighted not to result in deformation in the EO and, consequently, on the output point clouds.

4.4 Assessment of Exterior Orientation and Georeferencing

The residuals of the GCPs are provided by BBA, which indicate the difference between measured coordinates and newly calculated values. Errors in the photogrammetric network of observations are indicated by relatively large residual values. Large residuals in

GCPs were modified or deleted until an optimal solution has been found. The nature of these errors may be due to two different aspects: errors in the measurement of 3D coordinates of GCPs from satellite observations, or in the measurement of their 2D coordinates in the images.

Nevertheless, removing too many GCPs might reduce the photogrammetric model validity, especially if numerous parameters were to be estimated.

4.5 Dense Cloud Generation

Agisoft Metashape® software can create a dense point cloud based on the computed EOs and the photos themselves based on dense Multi-View Stereo (MVS) matching. The first step in the MVS process is the computation of *depth maps* on the basis of image disparities in normalized image pairs. In a second step, *depth maps* are used to generate a dense point cloud [18]. Multiple pairwise *depth maps* created for every camera are integrated into a combined *depth map*, with extra information in overlapping locations used to filter out incorrect depth measurements [14]. The camera's combined *depth maps* are turned out into partial dense point clouds, which are then blended into a final dense point cloud with further noise filtering done in overlapping locations. Subsequently, the dense cloud was modified to eliminate points that were not on continuous surfaces, such as supraglacial lakes, as well as visible outliers.

All procedures were carried out in a "high-quality" setting in Metashape®, which has been retained as the best compromise between the obtainable quality and the processing time.

5 Point-Cloud Analysis

Photogrammetric point clouds obtained from the archive aerial photos are utilized to compute the variations in glacier thickness between different epochs. In this paper we focus on the evolution of the Miage Glacier in the period from 1967 to 2006.

In order to compare point clouds, the open-source software package CloudCompare (www.cloudcompare.org) has been used. Prior to analysing cloud pairs, some preprocessing steps have been applied to improve data quality in different data sets. The first step is to eliminate all outliers and noisy points from each point cloud. One approach to generate a clean point cloud with a homogenous surface density, is to extract the related components using a 3D grid which is called Label Connected Component [30]. Another technique is S.O.R Filter/Noise Filter. These methods are fairly similar between them since they both eliminate points that are over a specific distance from the plane fitting a particular number of neighbours for each point (kNN) [12]. As a result, Label Connected Component is applied to each point cloud to remove outliers that are separated from the point cloud by a substantial distance, and S.O.R or Noise filter are applied if there are more noises near the surface of the point clouds.

Because each point cloud has been independently georeferenced in the national geodetic datum (RDN 2008.0/UTM32N), but this operation resulted in some residuals due to non-homogenous errors, a refinement of the co- registration between each pair of point clouds to compare has been applied in CloudCompare. Due to the vastness

of the area of interest, different approaches for co-registration have been examined. Indeed, point clouds to compare feature some unstable areas where changes occurred: these regions should not be considered to select control points for co-registration. Consequently, some stable areas have been selected and point clouds segmented to extract subsets there. The ICP (Iterative Closest Points – see Pomerleau et al. 2013 [25]) method for point cloud co-registration as implemented in CloudCompare has been applied. After a preliminary initial co-registration, that in this case was obtained from the use of GCPs in photogrammetric processing, the ICP techniques computes the rigid-body transformation which minimizes the distances between points in both point clouds to co-register. Here this process has been limited to the stable areas. Then the transformation parameters computed in this way have been applied to the remaining parts of both point clouds. Stationary regions in the model have been investigated to check out the quality of co-registration. To this purpose, the ICP distance between both clouds has been calculated in those regions.

After co-registration refinement, the M3C2 (*Multi-scale Model to Model*) technique has been applied to detect changes. M3C2 is well-suited to assessing statistically significant changes between point clouds where the geometry varies in three dimensions, and it is resistant to changes in point density and point cloud noise [20]. For example, in some studies where this method was used for estimating geomorphologic variations in channel sedimentation, M3C2 emerged as the most reliable method for highlighting erosion and deposition rates from point cloud comparisons, due to the fact that this procedure does not use interpolation, which might cause errors, particularly for complex landforms [17]. Therefore, M3C2 is considered as main method for comparison of data sets in this research.

5.1 Volume Computation

For the evaluation of volume change of glaciers between two epochs when photogrammetric point clouds were derived, CloudCompare implements a specific function to this purpose. This function derives the volume between two point clouds after selecting a reference plane, to be used for deriving 2.5D raster Digital Elevation Models (DEMs)[26]. The volume is derived from the computation of the DOD (DEM of Differences) between both DEMs to compare. Then the DOD is used to derive the volume by using the area of the grid step. The smaller the size of each elementary cell, the more accurate the computed volume. On the other hand, the grid step should be coherent with the density of the point cloud [4]. The percentage of average neighbours in each cell should be considered. It should be kept close to 8, or gaps would emerge between the cells, resulting in an incorrect volume estimation.

The percentage of cells in a DEM that have a matching cell in the second DEM shows how completely both point clouds overlap. Step size of generated grid should be optimized to make “Average neighbours per cell” as close as possible to 8. In all the comparison cases, the step value is optimized between 3 and 5 to obtain a value of 7.9 for the “Average neighbours per cell”. Due to importance of height difference in these comparisons, the projection direction for the volume calculation is considered to be the Z direction and the height of each cell is considered to be the average of the points inside the cell.

6 Result and Analysis

The approach described in Sect. 5 has been applied to process all datasets. For datasets including images from multiple cameras, a pre-calibration procedure is used before applying SfM/MVS algorithms in Agisoft Metashape®. With the exception of data from 1967, all data sets downloaded from the IGNF geoportal were provided with pixel size and focal length information. In addition, for image sets containing camera position GNSS coordinates, the SfM has been computed by using these data as starting camera locations. This resulted in reducing the time for computing the EO at the full image resolution (options: "high-quality" alignment precision and exclusion of stationary tie points). After the alignment process, the error of chosen GCPs is obtained for each dataset (Table 2). GCPs are chosen in a way that they have at least two projections on the images and are spread out as much as feasible throughout the whole region, avoiding weak configurations (Fig. 3).

Table 2. The root mean square error of GCPs in X-easting, Y-northing and Z-altitude for each dataset.

Year	X error (m)	Y error (m)	Z error (m)	XY error (m)	Total (m)
2006	1.293	0.704	1.380	1.473	2.018
2001	0.570	3.156	0.331	3.208	3.225
2000	1.328	2.429	0.679	2.768	2.850
1996	1.465	3.239	2.453	3.556	4.320
1988	1.486	4.300	0.693	4.550	4.603
1979	2.480	1.789	0.197	3.058	3.064
1967	0.218	0.941	0.939	0.965	1.347

For all the datasets except 2006 and 1967 photogrammetric blocks, fiducial marks have been used in the BBA. Then in this case the alignment procedure can be done either using fiducial marks or masking them. In most cases, masking the fiducials results in better alignment and denser point cloud. In 1996, 2000, and 2001 datasets camera location coordinates are available. The dataset from 1996 contains 35 photos from two separate cameras: 27 images taken with the RMK TOP 15 camera type, which has a calibration certificate, and 8 images taken with another camera, for which a calibration certificate was not available. The 8 photographs acquired by separate cameras will not be aligned with the other 27 images if the conventional methodology is followed, i.e., by measuring fiducial marks in photos. To overcome this issue, two groups are aligned independently in two chunks, and then the camera calibration properties exported from each other. Pre-calibration parameters will indeed be based on the calibration data of both groups of images. For the dataset from 1979, the calibration certificate allows the use of fiducial marks, but the camera coordinates are missing. This is the only dataset in which utilizing fiducial marks in the alignment operation results in an increased number of aligned images and a denser 3D model. In addition, in images of the dataset from

1967, because it is the oldest dataset in this study and because there is no corresponding calibration certificate, using fiducial marks has not been feasible, and they were masked.



Fig. 3. An example of reconstructed 3D dense cloud from the 2001 dataset representing the position and distribution of GCPs.

6.1 Assessing the Evolution of Miage Glacier

To compute the volume changes of glaciers over time, 3D surface models are compared. Thanks to GCPs, different photogrammetric blocks have been georeferenced in the same coordinate system, and then co-registration has been improved by exploiting overlap between pairs of point clouds. To ensure the quality and reliability of co-registration, points within five stable windows have been segmented and used for co-registration refinement based on ICP. Residual distances in these windows after this process have been adopted for the assessment of the co-registration accuracy (Table 3).

Table 3. Residual co-registration errors in five sample windows of stable parts around Miage Glacier.

Time period	Points in sample widows	Mean of M3C2 distances [m]	Standard deviation of M3C2 distances [m]	RMSE (root mean square error) of M3C2 distances [m]
2001–06	114k	1.31	1.61	2.82
2000–01	74k	0.90	2.60	2.70
1996–2000	158k	1.61	2.94	3.20
1988–96	218k	0.67	2.26	2.27
1979–88	230k	1.95	4.67	4.95
1967–79	128k	0.67	3.27	3.53

The accuracy of the co-registration resulted in a mean difference from 0.5 to 1.5 m (Table 2) and root means square error of distances varying between 2 and 5 m.

The evaluation of changes in glacier thickness has been done over an area of approximately 5 km^2 of the glacier tongue. The maximum average height reduction occurred between 2001 and 2006 with 3.5 m of decrease, while the variation is minimum from 2000 to 2001. Similarly, the largest volume changes mostly occurred from 2001 to 2006. In contrast, the only major increase of glacier thickness occurred in from 1979 to 1988. After 1988, the glacier started losing mass. Distribution of height variation of point clouds (Fig. 4) suggest mostly mass loss condition in Miage glacier through the decades and the last 5 years showed the largest contribution. The comparison between 2001 and 2006 shows that glacial mass loss occurred largely in the lower regions of the Miage tongue, whereas in 2000–01, the losses happened in the middle part, while the lower part showed little change. From 1996 to 2000, the volume and height decreased primarily in the lower half of the glacier tongue, with some gain was observed in the top half. In contrast, in the lower section of Miage glacier mass increased from 1967 to 1988. Due to huge shadows covering the middle sections of Miage in the photos of the dataset of

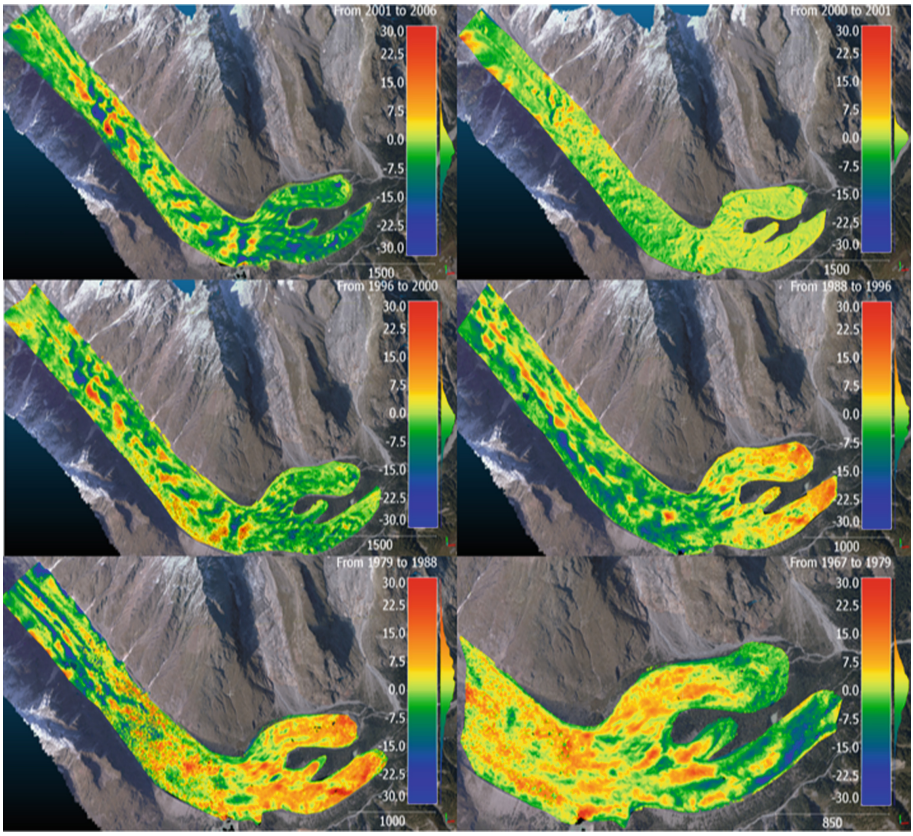


Fig. 4. Miage Glacier evolution and distribution of mass loss in glacier from year 1967 to 2006.

1967, the 3D model of this dataset has numerous outliers and noise in the middle part of Miage glacier tongue, and only the bottom half of Miage is considered for comparison in the 1967 point-cloud. Overall, the Miage glacier experienced a slight mass gain until 1988, then a gradual decrease in thickness over time, although not abrupt. In addition, the rate of mass loss tends to rise over time. Similarly, the thickness of the upper branches of Miage has remained consistent, with the exception of 2000, when a high retreat rate of −3 m per year was observed, resulting in a decrease in height.

Furthermore, the volume variation calculation throughout the years when cloud pairs are compared may be used to calculate the Miage glacier mass loss rate, by subtracting the volume of the glacier from two distinct point clouds and taking the surface area into account. This method allows us to comprehend the fluctuation of the Miage across all years until 2006, not only during the time that datasets are available (Fig. 5).

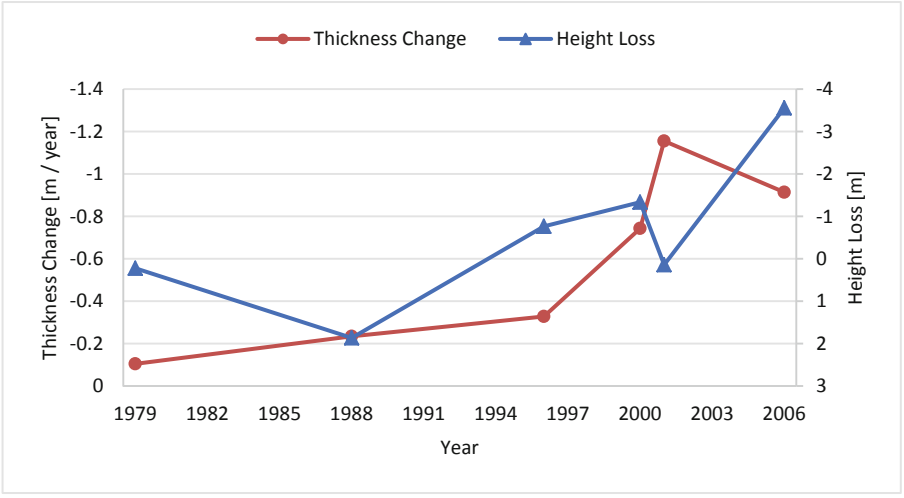


Fig. 5. Mean height and thickness change rate variation of Miage glacier in Val Veny through the years.

7 Conclusions

Archival photographs were utilized in this research to better understand the evolution and dynamics of Miage glacier in Val Veny from 1967 to 2006. Photogrammetric methods can be used to interpret morphological change captured in a sequence of aerial photographs. These data were acquired by IGNF (National Geographic and Forestry Institute of France) and covered an area ranging from 132 to 345 km^2. The data were acquired with various airborne cameras during the warmer months of the year. To understand the variation of Miage glacier through these years, 3D models obtained from these data were compared. The 3D model of each series of photos was reconstructed using the Structure-from-Motion technique followed by dense Multi-View Stereo matching. Some

pre-processing was conducted before the main procedure to improve keypoint extraction from photographs. According to availability of calibration certificates for some datasets, it was possible to try the alignment procedure by using fiducial markers. However, in most of the datasets, masking the fiducial markers leads to better or equivalent results. Satellite data was used to identify stable points that were used as GCPs in all images, resulting in improved initial alignment of the 3D models during the comparison phase. The appearance of shadows on the glacier in some zones is due to the presence of high cliffs and improper photography timing, and this fact leads to missing data in some portions of the 3D model.

To use 3D models to investigate variations in Miage glacier, noise must be filtered and model alignment must be accurate enough to provide an accurate result. The distances between the stable zones may be used to measure the co-registration quality between two point clouds. The error in the co-registration procedure may be evaluated in the mean distances in stable areas after co-registration refinement based on ICP. The registration error varies depending on the quality of the 3D model in different zones of Val Veny, but it is usually between 1 and 2 m. *Multi-scale Model to Model* (M3C2) method for cloud comparison was employed to determine distances, as recommended by prior studies, especially for complex landforms.

In the Miage Glacier, height loss was determined to be 1 m/y between 2000 and 2006, after being almost negligible until the 1990s. however there is a general increasing trend in both height and volume loss from 1979 to 2006. Furthermore, the findings of this study may be integrated with more contemporary models acquired by using more advanced photogrammetry technology to assess whether the variations in Miage glacier follow the same trend as before. The methodology applied in this research may be transferred to various applications or locations if archival photographs are available. Unidentified causes of natural disasters, including landslides, floods, and droughts, can be identified by analysing archival photographs of the region and using the results for risk mitigation and planning in the long term.

References

1. Aguilar, M., Aguilar, F., Fernandez, I., Mills, J.: Accuracy assessment of commercial self-calibrating bundle adjustment routines applied to archival aerial photography. Photogram. Rec. **28**(141), 96–114 (2013)
2. Azzoni, R.S., et al.: Recent structural evolution of Forni Glacier tongue (Ortles-Cevedale Group, Central Italian Alps). J. Maps **13**(2), 870–878 (2017). https://doi.org/10.1080/17445647.2017.1394227
3. Baumann, P.: Aerial Photography: History and Georeferencing. The Geographic Information Science & Technology Body of Knowledge, 2nd Quarter edn. (Ed. by, J.P. Wilson) (2019)
4. Costa, J.E.: Physical geomorphology of debris flows. In: Costa, J.E., Fleisher, P.J. (eds.) Developments an Applications of Geomorphology, pp. 268–317. Springer, Berlin (1984). https://doi.org/10.1007/978-3-642-69759-3
5. Cox, S.C., et al.: Rock avalanche on 14 July 2014 from Hillary Ridge, Aoraki/Mount Cook, New Zealand. Landslides **12**(2), 395–402 (2015). https://doi.org/10.1007/s10346-015-0556-7
6. De Michele, C., et al.: Using a fixed-wing UAS to map snow depth distribution: an evaluation at peak accumulation. Cryosphere **10**, 511–522 (2016)

7. Deline, P.: Etude géomorphologique des interations écroulements rocheux/glaciers dans la haute montagne alpine (versantsud-est du massif du Mont Blanc). Thèse de doctorat de géographie, Université de Savoie, p. 539 (2002)
8. Eltner, A., Kaiser, A., Castillo, C., Rock, G., Neugirg, F., Abellán, A.: Image-based surface reconstruction in geomorphometry – merits, limits and developments. Earth Surf. Dyn. **4**, 359–389 (2015)
9. Fey, C., Wichmann, V., Zangerl, C.: Reconstructing the evolution of a deap seated rock-slide (Marzell) and its responseto glacial retreat based on historic and remote sensing data. Geomorphology **298**, 72–85 (2017)
10. Fox, A.J., Cziferszky, A.: Unlocking the time capsule of historic aerial photography to measure changes in Antarctic Peninsula Glaciers. Photogramm. Rec. **23**(121), 51–68 (2008)
11. Fraser, C.S.: Automatic camera calibration in close range photogrammetry. Photogramm. Eng. Remote. Sens. **79**(4), 381–388 (2013)
12. Fugazza, D., et al.: Combination of UAV and terrestrial photogrammetry to assess rapid glacier evolution and map glacier hazards. Nat. Hazards Earth Syst. Sci. **18**, 1055–1071 (2018). https://doi.org/10.5194/nhess-18-1055-2018
13. Fugazza, D., et al.: Highresolution mapping of glacier surface features. The UAV survey of the Forni Glacier (Stelvio National Park, Italy). Geografia Fisica e Dinamica del Quaternario **38**, 25–33 (2015)
14. Giordano, S., Le Bris, A., Mallet, C.: Fully automatic analysis of archival aerial images current status and challenges. In: Joint Urban Remote Sensing Event (JURSE) (2017)
15. Haala, N., Kada, M.: An update on automatic 3D building reconstruction. ISPRS J. Photogramm. Remote Sens. **65**, 570–580 (2010)
16. Huggel, C.: Recent extreme slope failures in glacial environments: effects of thermal perturbation. Quat. Sci. Rev. **28**, 1119–1130 (2009)
17. James, M.R., Robson, S., Smith, M.W.: 3-D uncertainty-based topographic change detection with structure-from-motion photogrammetry: precision maps for ground control and directly georeferenced surveys. Earth Surf. Proc. Landforms **42**(12), 1769–1788 (2017)
18. Kaufmann, V.; Ladstädter, R.: Quantitative analysis of rock glacier creep by means of digital photogrammetry using multitemporal aerial photographs: two case studies in the Austrian Alps. In: Proceedings of the 8th International Conference on Permafrost, Zurich, Switzerland, 21–25 July 2003, pp. 21–25 (2003)
19. Koblet, T., et al.: Reanalysis of multi-temporal aerial images of Storglaciären, Sweden (1959–99) – Part 1: determination of length, area, and volume changes. Cryosphere **4**, 333–343 (2010). https://doi.org/10.5194/tc-4-333-2010
20. Kraus, K.: Photogrammetry - Geometry from Images and Laser Scans. Walter de Gruyter, Berlin (2008)
21. Lague, D., Brodu, N., Leroux, J.: Accurate 3D comparison of complex topography with terrestrial laser scanner: application to the Rangitikei canyon (N-Z), ISPRS J. Photogramm. Remote Sens. (2012)
22. Micheletti, N., Chandler, J.H., Lane, S.N.: Section 2.2. Structure from Motion (SfM) photogrammetry. In: Cook, S.J., Clarke, L.E., Nield, J.M. (eds.) Geomorphological Techniques (Online Edition), pp. 2047–2371. British Society for Geomorphology, London (2015)
23. O'Connor, J.E., Costa, J.E.: Geologic and hydrologic hazards in glacierized basins in North America resulting from 19th and 20th century global warming. Nat. Hazards **8**, 121–140 (1993)
24. Poli, D., Casarotto, C., Strudl, M., Bollmann, E., Moe, K., Legat, K.: Use of historical aerial images for 3d modelling of glaciers in the Province of Trento. ISPRS Int. Arch. Photogramm. Remote Sens. Spat. Inf. Sci. **XLIII-B2**, 1151–1158 (2020)
25. Pomerleau, F., Colas, F., Siegwart, R., Magnenat, S.: Comparing ICP variants on realworld data sets. Auton. Robot. **34**, 133–148 (2013)

26. Scaioni, M., Roncella, R., Alba, M.I.: Change detection and deformation analysis in point clouds: application to rock face monitoring. Photogramm. Eng. Remote. Sens. **79**(5), 441–456 (2013)
27. Scaioni, M., et al.: Structure-from-motion photogrammetry to support the assessment of collapse risk in Alpine Glaciers. In: Altan, O., Chandra, M., Sunar, F., Tanzi, T. T. (eds.) Gi4DM 2018. LNGC, pp. 239–263. Springer, Cham (2019). https://doi.org/10.1007/978-3-030-05330-7_10
28. Scaioni, M., Corti, M., Diolaiuti, G., Fugazza, D., Cernuschi, M.: Local and general monitoring of Forni glacier (Italian alps) using multi-platform structure-from-motion photogrammetry. Int. Arch. Photogramm. Remote Sens. Spat. Inf. Sci. **42**(Part 2/W7), 1547–1554 (2017). https://doi.org/10.5194/isprs-archives-XLII-2-W7-1547-2017
29. Scaioni, M., et al.: Technical aspects related to the application of SfM photogrammetry in high mountain. Int. Arch. Photogramm. Remote Sens. Spat. Inf. Sci. **XLII**(Part 2), 1029–1036 (2018)
30. Schneider, D., Huggel, C., Cochachin, A., Guillén, S., García, J.: Mapping hazards from glacier lake outburst floods based on modelling of process cascades at Lake 513, Carhuaz, Peru. Adv. Geosci. **35**, 145–155 (2014). https://doi.org/10.5194/adgeo-35-145-2014
31. Smiraglia, C., Diolaiuti, G., D'Agata, C.: I ghiacciai delle Alpi italiane: variazioni areali e volumetriche e dinamica geomorfologia recente. Relazione contratto di ricerca n8 R1877. CESI, Milano (2001)
32. Smiraglia, C., Diolaiuti, G., Casati, D., Kirkbride, M.: Recent areal and altimetric variations of Miage Glacier (Monte Bianco Massif, Italian Alps). In: Nakawo, M., Raymond, C.F., Fountain, A. (eds.) Debris-Covered Glaciers, vol. 264, pp. 227–233. IAHS Publ. (2000)
33. Tavakoli, K., Zadehali, E., Malekian, A., Darsi, S., Longoni, L., Scaioni, M.: Landslide dam failure analysis using imaging and ranging sensors. In: Gervasi, O., et al. (eds.) ICCSA 2021. LNCS, vol. 12955, pp. 3–17. Springer, Cham (2021). https://doi.org/10.1007/978-3-030-87007-2_1
34. Walstra, J., Dixon, N., Chandler, J.H.: Historical aerial photographs for landslide assessment: two case histories. Quart. J. Eng. Geol. Hydrogeol. **40**, 315–332 (2007)
35. Westoby, M.J., Brasington, J., Glasser, N.F., Hambrey, M.J., Reynolds, J.M.: 'Structure-from-motion' photogrammetry: a low-cost, effective tool for geoscience applications. Geomorphology **179**, 300–314 (2012). https://doi.org/10.1016/j.geomorph.2012.08.021